# Three-Dimensional Numerical Investigation of Tunnel Behavior Based on Different Constitutive Models and Associated Parametric Analysis in Rock Medium

Sepehr Chalajour[a], Nader Hataf*[b]

[1]Department of Civil Engineering, Shiraz University, Shiraz, Iran

[2]Department of Civil and Environmental Engineering, Shiraz University, Shiraz, Iran

## Abstract

With the advancement of numerical modeling, predicting tunnels' behavior before construction has become possible for designers. Accurate prediction of tunnels' behavior in diverse environments requires the compatibility of numerical simulations with ground conditions. Although several constitutive models have been proposed for simulating ground characteristics, their appropriate utilization is crucial. In this study, the convergence of a tunnel was modeled, and the results were verified using actual convergence monitoring data. Then, a series of finite element simulations were conducted on a hypothetical TBM tunnel to demonstrate the difference in deformations, ground surface settlements, and stresses in the lining resulting from tunnel excavation under seven constitutive models in rock media. The models were categorized into four groups: rock-specified, soil-established, and general. Additionally, parametric studies were performed on specific gravity, Poisson's ratio, and dilation angle. The findings revealed that different constitutive models significantly influence numerical analysis results. Rock-specified models were found to be more sensitive to parameter variation in rock media than soil-established and general models. Moreover, changes in specific gravity and Poisson's ratio had a significant impact on the magnitude of surface settlements. Overall, the study highlights the importance of appropriately selecting constitutive models and accurately defining material parameters in numerical simulations to ensure reliable predictions of tunnel behavior.

[a] Graduate student
Email: sepehrchalajour@gmail.com
[b] Corresponding Author, Ph.D., Professor
Phone: +98 71 3613 3108, Telefax: +98 71 3647 3303
Email: nhataf@shirazu.ac.ir

## 1. Introduction

The rapid growth of urban areas in recent decades has resulted in the construction of numerous structures and infrastructures, including tunnels. Tunnels are critical underground structures used for various purposes such as transportation, access roads, powerhouse caverns, and water transition ducts (Audi et al. 2020). Consequently, it is crucial to accurately predict their behavior during the design phase. The behavior of tunnels can be evaluated by analyzing the crown settlement, ground surface settlement, and the stresses that develop on the lining system. Reliable predictions of tunnel behavior are necessary to ensure the safety and durability of the structure, as well as to avoid potential damages and costs associated with unforeseen events. Therefore, it is essential to utilize advanced numerical modeling techniques and appropriate constitutive models to accurately simulate the behavior of tunnels in different environments.

Excavation of a tunnel at any depth in the ground causes a redistribution of stresses, which affects the support system of the tunnel and causes displacement in the surrounding area. Accurate prediction of tunnel behavior is essential to optimize the design of the support system (Hajiazizi et al. 2021). In addition, ground surface settlement resulting from deformations can cause damage to structures located at the ground level. Several studies have been conducted to evaluate the displacement and stress distribution in the tunnel environment and the tunnel support system. These studies can be classified into three categories: empirical, analytical, and numerical methods. Empirical methods typically express the deformations and stresses developed in tunnel structures using empirical equations. These equations are a mathematical language that describes the behavior of the tunnel in terms of a series of variables and logical and quantitative relationships between these variables. Empirical equations are typically developed based on field measurements and observations, and they often incorporate simplifying assumptions to make them more practical and easier to apply. While empirical methods can be useful for quickly estimating the behavior of tunnels, they are often less accurate than analytical or numerical methods, which can take into account a wider range of factors and provide more detailed results. Analytical methods involve using mathematical models to predict the behavior of the tunnel based on simplified assumptions. These methods simplify complex tunnel problems by making certain assumptions, which then allow for the derivation of theoretical equations to calculate stresses and deformations. These assumptions can include the homogeneity and isotropy of the tunnel lining, or that stresses and deformations are only a function of the radial distance from the tunnel center. While analytical methods can provide useful insights into tunnel behavior, they may not be as accurate as numerical methods which can consider a wider range of factors and provide more detailed results. Kirsch's solution to determine the stresses surrounding a tunnel in an elastic environment is this kind (Goodman, 1989). Pinto (1991) developed an analytical solution to describe the curvature shape of surface settlement. Bobet (2001) studied 28 tunnels and suggested an analytical approach based on ignoring the time-dependent material behavior to calculate the ground deformations induced by tunnel excavation in saturated shallow depths. Bakker (2003) proposed several equations to compute axial forces, flexural moments, and radial displacements of a tunnel. Park (2004) presented an analytical method to calculate tunnels' elliptical deformations in clays by modifying the Bobet equations and elastic theory. Numerical methods, such as finite element analysis, use complex mathematical models to simulate the behavior of the tunnel and surrounding ground in great detail. From studies that have investigated the influence of constitutive models on tunnel's response, Oettl et al. (1998), Hejazi et al. (2008) and Rukhaiyar and Samadhiya (2016) can be named. Chen and Lee (2020) researched tunnel deformation by three-dimensional (3D) finite element (FE) analysis in horseshoe-shaped tunnels under various geological conditions by Mohr-Coulomb and Hoek-Brown constitutive models. They showed that the predicted deformations by the two models are close. Chalajour and Hataf (2022) investigated the most appropriate constitutive model for each rock category based on the strength parameters based on the actual behavior of two tunnels.

The problem associated with design and analyzed is the lack of knowledge in the nonlinear behavior of structure and soil interaction, affecting the magnitude of stresses (Shid Moosavi and Rahai, 2018). Zhao et al. (2017), Beyabanaki and Gall (2017) performed a series of parametric studies on different characteristics of soil and the tunnel itself to investigate the effect of modulus of elasticity, construction steps, horizontal to vertical stress ratio, tunnel angle and, tunnel diameter on tunnel behavior. Yoo (2016) conducted a series of 3D FE parametric studies on several tunnel cases and indicated that displacements at the tunnel crown and sidewalls could be related to the weak zone's spatial characteristic and the initial stress state. Ding and Liu (2018) investigated the effect of tunnel burial depth, tunnel diameter and lateral pressure coefficient on the stress and deformation of tunnel surrounding rock under sandstones. Jallow et al. (2019), by 3D analyzing a TBM tunnel, investigated the effect of different soil constitutive models, the agreement of surface settlement calculations and monitoring, and parametric analysis of the impact of various parameters on long-term settlements. Zheng et al. (2017) investigated the unloading effect due to the tunnel excavations by considering the small strain characteristics of soil and showed it could cause adjacent tunnels' deformation. Wang et al. (2019) studied the effect of constructing a large diameter shallow buried twin tunnel in soft soil on the ground surface settlement. They showed the range of the longitudinal surface settlement affected by the tunnel excavation face for different soft soils. Anato et al. (2021) investigated the effect of the shield-driven speed, modulus of elasticity of grout, and the stiffens of the tunnel lining on ground surface settlement. They demonstrated that the ground surface settlement is considerably influenced by the tail void grouting properties and stiffness of tunnel lining. Various studies also for the assessment of the deformations due to tunnel excavation by comparing with data monitoring, have also been reported in the literature Aksoy and Uyar (2017), Su et al. (2019), Xing et al. (2018), Jin et al. (2020), Sun et al. (2020), Li et al. (2020), Ranjbarnia Su et al. (2020), Xue et al (2021) and Yang and Xu (2021).

Numerous studies have examined ground surface settlements resulting from tunnelling and the associated stresses on the lining and deformations, however, most of these studies have focused solely on the soil medium. Consequently, a gap exists in the literature regarding the evaluation of tunnel behavior under different constitutive models in rock mediums. Additionally, parametric studies have been overlooked in some previous investigations. This paper aims to address these shortcomings by utilizing three-dimensional numerical modelling based on the rock mass rating (RMR) classification system proposed by Bieniawski (1973), with seven distinct constitutive models in four rock categories (very weak, weak, medium, and strong) typically utilized in tunnel analysis. By doing so, this study provides an understanding of the significant impact of selected behavior models and associated parametric studies on accurate results. By providing a better understanding of predicting and assessing tunnel behavior before construction, this study offers insight for engineers and can help improve tunnel design and construction.

## 2. Constitutive Models

Constitutive models provide a mathematical framework for describing the behavior of materials under different loading conditions. By using a single set of model constants, constitutive models enable predictions of how materials, such as soil and rock, will respond to stress paths of varying complexity. These models maintain constant parameters, irrespective of the stress path, and allow for state parameters to be adjusted during the analysis process. Thus, constitutive models provide a means of defining the relationship between stress and strain, enabling the calculation of incremental strains resulting from changes in stress. The Finite Element (FE) method incorporates material properties through the use of a defined constitutive model. This study explores the impact of seven different constitutive models, which include linear elastic (LE) and von Mises (VM) as general models, Mohr-Coulomb (MC), Drucker-Prager (DP), and Strain Softening (SS) as classical soil models, and Generalized Hoek-Brown (GHB) and Generalized Hoek-Brown with residual (GHBR) as special rock models for analysis. The following section briefly describes the selected models, but additional information on their behavior can be found in the references.

### 2.1. Linear Elastic model

The elastic behavior of a material can be linear or nonlinear. In linear elasticity, the elastic material properties are constants, but in nonlinear elastic models, they change based on some assumptions. In the LE model, the stress is linearly correlated with the strain, and the elastic properties are constants, represented as Hooke's Law, Eq. (1):

$$\sigma = E\varepsilon \qquad\qquad (Eq.1)$$

where E is Young's modulus of the material, and $\sigma$ and $\varepsilon$ are the stress and strain, respectively. The model's constants are Young's modulus and Poisson's ratio. This model does not define a failure criterion.

## 2.2. von Mises model

In the VM model, the yield occurs when the second invariant of the deviatoric stress tensor (q) reaching a critical value. This model is mostly used to simulate the ductile behavior of the material. When the VM model is applied to a soil material, the effect of hydrostatic pressure is not considered, and the yield surface is the same for both tension and compression (Davis and Selvadurai, 2005). It can be assumed that the material response is nonlinear elastic, viscoelastic or linear elastic prior to yielding. VM yield formulation is expressed as Eq. (2):

$$q = k \qquad\qquad (Eq.2)$$

where q is the deviatoric stress and k is the material's yield stress in pure shear respectively. VM criterion is formulated in terms of the von Mises stress or equivalent tensile stress. The first term predicts the yielding of materials under complex loading from the results of uniaxial tensile tests. On the other hand, the von Mises stress satisfies the property where two stress states with equal distortion energy have an equal von Mises stress.

## 2.3. Mohr-Coulomb model

The specification of MC model and associated yield criterion typically involve the hypothesis proposed by Coulomb, which postulated a linear relationship between shear strength on a plane and the normal acting stress on the p-q plane. This elastic-perfectly plastic model is one of the most commonly used and well-suited for evaluating geotechnical problems describing the conditions for which an isotropic material will fail, with any effect from the intermediate principal stress $\sigma_{II}$ being neglected. Mechanical behavior of the model includes features such as isotropic shear strength for the peak and residual, tensile strength, dilatancy and the shear strength dependency on Lode's angle. MC model is also being implemented to evaluate load-displacement magnitudes in the simulations, including geomaterials such as gravels, sands and rocks (Davis and Selvadurai, 2005). This model possesses five parameters to express behavior. Two parameters are adopted from Hooke's law (i.e., modulus of elasticity, E, and Poisson's ratio, $v$), two parameters to express the failure criterion (angle of internal friction, $\phi$, and cohesion, c) in addition to another parameter (dilation angle, $\psi$) that should be less than or equal to the (residual) friction angle which makes the flow rule non-associated or associated respectively, for determining the plastic volume change due to shear stress (Ng et al., 2015). MC criterion is written as Eq. (3):

$$\tau = c + \sigma tan\phi \qquad\qquad (Eq.3)$$

where $\tau$ and $\sigma$ are the shearing and normal stress (positive tension) on the physical plane through which material failure occurs, respectively. $\phi$ is also the angle of internal friction and $c$ represents the cohesion value in this model.

## 2.4. Drucker–Prager model

DP is a modification of VM model by introducing a dependence on the mean stress p according to Eq. (4). Constant parameters $\xi$ and k could be selected such that the model agrees with the Coulomb surface. This model is intended to simulate cohesive geological materials exhibiting pressure-dependent yield, including soils and rocks.

$$q - \xi p = k \qquad (Eq.4)$$

where q and k are the material properties representing peak and residual strength values. P is also defined as hydrostatic confinement. Similar to the MC criterion, this model simulates the elastic-perfectly plastic behvaior ; however, unlike the MC, which has the hexagonal yield surface on the deviatoric stress plane, the yield surface of the DP model in two and three-dimensional stress space is a line and a conical shape respectively. (Davis and Selvadurai, 2005).

## 2.5. Strain Softening model

Several studies have shown that the peak and residual strengths of rocks increase with an increase in confining pressure. Conversely, at lower confining pressures, the loss of the cohesive strength component around peak load leads to strain localization, resulting in significant stress drop - this is commonly referred to as strain-softening behavior (Rummel and Fairhurst, 1970). Cohesion parameters in the Strain Softening (SS) model vary with plastic strain rate, allowing for a piecewise linear definition of the stress-strain relationship. The yield criterion, potential function, plastic flow rule, and stress correction in the SS model are similar to the Mohr-Coulomb (MC) criteria. The SS model is implemented in the numerical modeling process after material yielding. The unit's new shear strength parameters are calculated based on the plastic strain at each iteration step, and the parameters are updated using a nonlinear equation between the shear strength parameter and plastic strain, before being used in the next iteration step. Through this cycle, the strain-softening behavior of rocks can be reflected (Li et al., 2019). Strain-softening (SS) refers to the deterioration of material strength as the strain increases. This model includes a linear component until the peak shear strength value is reached, after which failure occurs, and shear strength reduces to the residual shear strength. Softening behavior occurs when the stresses in the rock mass around the tunnel exceed the compressive stresses and gradually reduce to the residual strength with an increase in strain. The SS model features three nonlinear parameters that define its strain-softening behavior: Peak Cohesion ($C_p$), Residual Cohesion ($C_r$), and Softening Rate (R) (MIDAS Information Technology Co., 2018).

## 2.6. Generalized Hoek-Brown model

Hoek-Brown criterion is an elastic-brittle-plastic material model utilized to evaluate the failure criteria based on strength and deformations for rock masses. This model was introduced based on an attempt to provide input data for the analyses required for the design of underground excavations in hard rock, derived from the results of studies of the brittle failure of intact rock by Hoek (1968) and on model studies of jointed rock mass behavior by Brown (1970). This criteria idea commences from the features of intact rock, and then applying reduction factors based on the characteristics of joints in a rock mass is modified to suit the rock mass behavior. Mechanical behavior of the model is similar to the mechanical behavior of the MC criteria. Three different rock mass characteristics should be defined as input parameters of this model. The Uniaxial compressive strength of intact rock, $\sigma_{ci}$, Hoek-Brown constant value for rock mass, $m_i$, and Geological Strength Index, GSI, for rock mass. The modified Hoek-Brown equation is defined by Eq. (5), Eq. (6) and Eq. (7):

$$\sigma_1 = \sigma_3 + \sigma_{ci} \left( m_b \frac{\sigma_3}{\sigma_{ci}} + s \right)^a \qquad (Eq.5)$$

$$m_b = m_i \exp\left( \frac{GSI - 100}{28 - 14D} \right) \qquad (Eq.6)$$

$$a = 0.5 + \frac{1}{6} \left( e^{-GSI/15} - e^{-20/3} \right) \qquad (Eq.7)$$

Where, $\sigma_1$ and $\sigma_3$ are maximum and minimum principal stresses, respectively. $m_b$ is the Hoek-Brown constant parameter for rock mass, and a and s are dimensionless parameters which are dependent on the rock mass Geological Strength Index (GSI). GSI system represents the rock structure and block surface conditions. The GSI was introduced by Hoek, Wood and Shah (1992) and Hoek, Kaiser and Bawden (1995) in order to evaluate the mass rock strength from the intact rock properties. D is also the disturbance factor as a result of blast or stress relaxation. This parameter ranged from 0.0 for undisturbed in-situ rock mass to 1.0 for very disturbed

rock mass. Hoek-Brown parameters can be connected to the MC criteria parameters through some proposed correlations (Yasitli, 2016, Hoek and Brown, 2019)

## 2.7. Generalized Hoek-Brown with residual model

The residual behavior is calculated from substituting the $GSI_{Peak}$ instead of $GSI_{Residual}$ in the Hoek-Brown model (Russo et al.1998). This model behaves similarly to the SS model and calculates smaller residual values than the peak values according to the plastic softening of rocks. In the design of underground excavations, the post-peak behavior of rocks shows essential effect on the excavation stability (Cai et al. 2007). Concerning the recommended behavior range based on GSI, rock masses with GSI >75 show brittle behavior, 25 < GSI < 75 have softening behavior, and GSI < 25 exhibits complete plastic behavior (Lazemi and Soleiman Dehkordi, 2019, Hoek and Brown, 1997). The determination of residual parameters based on Hoek-Brown criteria was discussed by He et al., 2020. For this study, the residual value of the GSI calculated from the empirical equation Eq. (8) proposed by Russo et al. (1998).

$$GSI_{residual} = GSI.e^{-0.134GSI}$$ (Eq.8)

# 3. Verification of Numerical Modeling

## 3.1. Numerical Modeling

To evaluate the influence of constitutive models and associated parametric studies in predicting tunnel behavior, a three-dimensional (3D) modeling approach was employed for numerical simulations. The MIDAS GTS NX 2018, a Finite Element (FE) simulation program specifically designed for geotechnical analysis, was used for the computational resource in this research. This software is capable of modeling porous media, including rock and soil.

## 3.2. Case study - Isfahan-Shiraz Railway Tunnel

The selected case study to verify the accuracy of the result obtained from the software, Isfahan-Shiraz railway tunnel monitoring data and field characteristics report were adopted. The tunnel has a horseshoe-shaped cross-section, with an approximate length, height and width of 820 m, 5.75 m, and 8.2 m, respectively. On December 19th, 2006, the B1-1 monitoring convergence station was situated at 269 + 047.5 kilometres, located at a distance of about 717.5 meters from the tunnel entrance. The tunnel overburden at this station is 29 meters, and the material types are mostly shale and sandstone. The tunnel's temporary support system consists of two layers of wire mesh, 25 cm thick shotcrete, and a steel frame (Sarikhani Khorami, 2012).

In the numerical simulation, the support system modeled as an equivalent shotcrete thickness and the tunnel excavation and base shotcrete application were simultaneously performed in a single stage. Elastic modulus, cohesion, internal friction angle, and lateral pressure coefficient of the tunnel medium are shown in Table 1. Parameters were calculated through the back analysis based on MC criteria by considering a constant value for Poisson's ratio and specific gravity. The calculated parameters represent the ground condition of the tunnel's environment. The adapted method to back analysis was performed by constant consideration of parameters in the reasonable range for the existing ground. Then other parameters were changed in a range to obtain the best match quality with the recorded monitoring data.

Table 1. Ground Parameters for Isfahan-Shiraz Railway Tunnel

| Modulus of Elasticity (MPa) | Cohesion (kPa) | Angle of Internal Friction (deg.) | Lateral Pressure Coefficient | Poisson's Ratio | Unit Weight (kg/m³) |
|---|---|---|---|---|---|
| 321 | 112 | 16.15 | 2.48 | 0.25 | 2400 |

Based on the method proposed by Singh and Goel. (1999), 98% of the total tunnel displacements occur up to two times the tunnel diameter from the tunnel's face as a result of the tunnel face's advancing. In this zone, the rock mass's time-dependent behavior does not significantly impact the convergence of the tunnel face (Asadollahpour et al., 2014). Fig. 1 shows the comparison of the tunnel walls' convergence monitoring data and the outcome of the performed FEM analysis at the B1-1 station. Numerical modeling results had a good agreement with the reported convergence value of the tunnel.
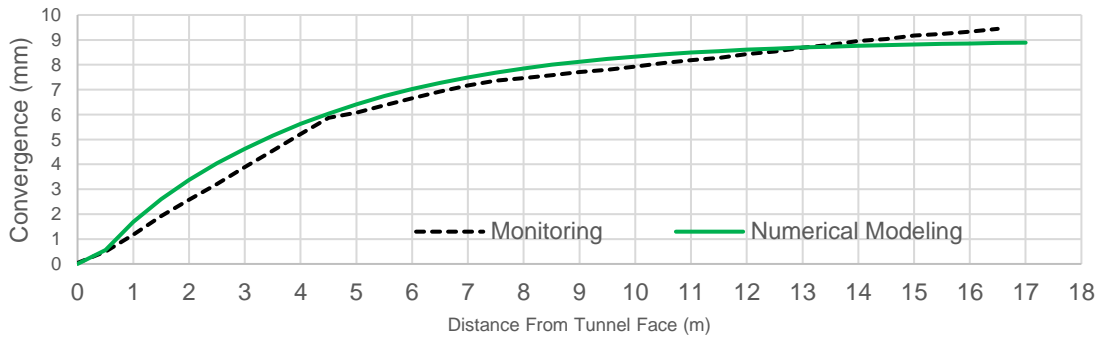


Fig. 1. Comparison of the results of Isfahan-Shiraz Railway Tunnel numerical modeling and monitoring

## 4. Numerical Modeling

In numerical modeling, the tunnel was modelled with a radius of 4.25 m, a depth of 36 m and a lining thickness of 25 cm. The dimensions of the model are 99m × 85.5m × 108m, which was considered greater than five times the tunnel diameter at the sides (Vitali et al 2018), and 12 times greater than the tunnel diameter in the longitudinal direction (Carranza-Torres et al. 2013). Also, the tunnel face is located at a distance of 6 times the diameter (54 m) from the tunnel's beginning. Fig. 2 shows the geometry and mesh elements of the simulated model.
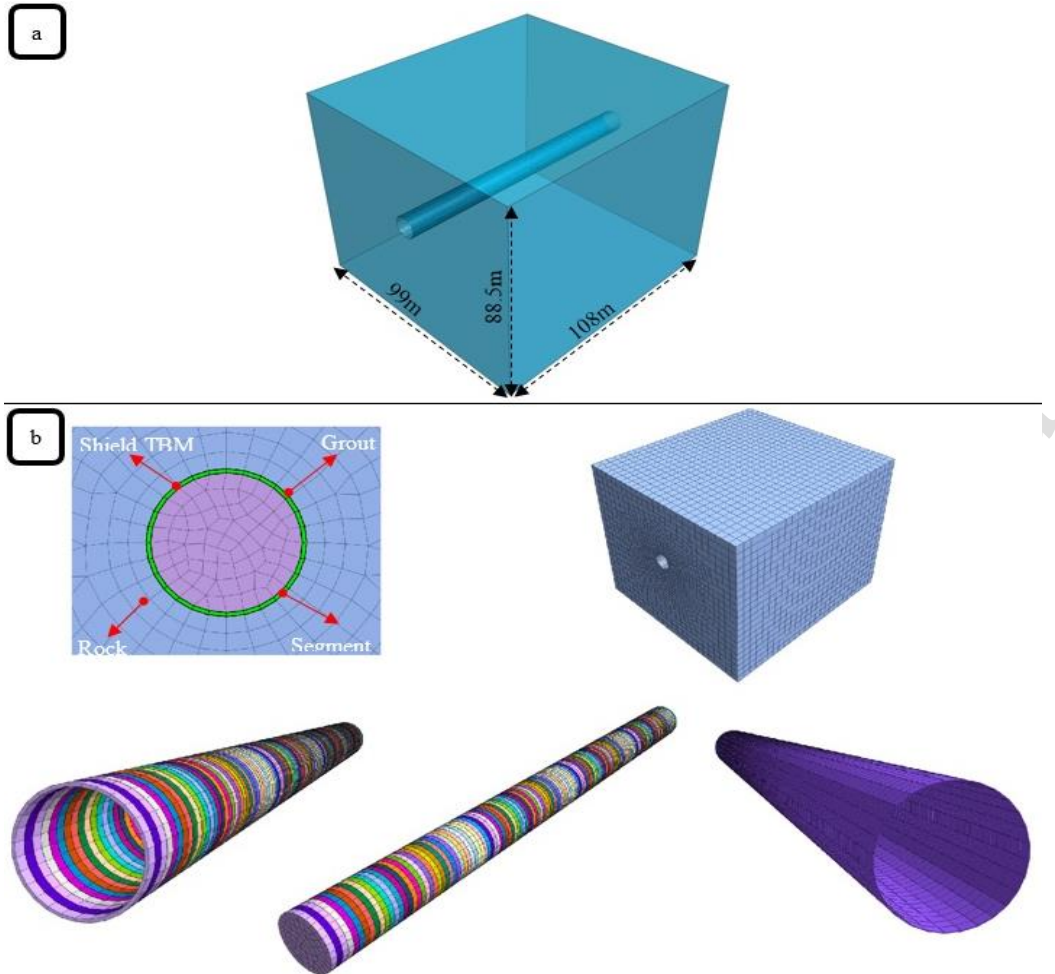
Fig. 2. a) Geometry and b) the FE mesh

To accurately simulate the behavior of a typical TBM tunnel during construction, the numerical modeling considered the actual procedure and sequences involved in the construction process, such as drilling, installing steel shields, installing segments, grouting, and applying jack and face pressures. Solid elements were used to model the rock medium and concrete segments of the tunnel, while shell elements were employed to simulate the steel shield and grout. The concrete segments, steel shields, and grout were defined as elastic materials. The rock mass behavior was investigated using seven constitutive models: LE, VM, MC, DP, SS, GHB, and GHBR. The boundary condition of the model involved restraining the model in the horizontal directions as a roller on all sides, and the bottom part of the mesh was pinned and restrained in the horizontal and vertical directions. Table 2 summarizes the characteristics of the tunnel support system in numerical modeling. Also the numerical modeling steps were conducted as the following steps:

- Defining the geometry of the model.
- Defining the material constitutive model and support system material parameters.
- Incorporating the excavation and support system in the geometry of the model.
- Defining the boundary conditions and generating the mesh.
- Defining the analysis sequence in the mesh of the model, including the stage construction sequence of applying the in-situ condition, ground excavation, and application and activation of the tunnel support systems.
- Performing the analysis.
- Assessing the results

Table 2. Characteristics of the tunnel support system in numerical modeling

| Name | Shield | Grout | Segment |
|---|---|---|---|
| Model Type | Elastic | Elastic | Elastic |

| | | | |
|---|---|---|---|
| Thickness (Cm) | 5 | 5 | 25 |
| Elastic Modulus (kPa) | $2.1 \times 10^8$ | $1 \times 10^7$ | $2.2 \times 10^7$ |
| Poisson's Ratio | 0.2 | 0.3 | 0.3 |
| specific gravity ($\frac{kN}{m3}$) | 78 | 22.5 | 24 |

To investigate the behavior of the tunnel under different constitutive models, the rock mass has been classified from very weak to strong groups based on strength and the suggested groups by Singh and Goel (1999). Table 3. Indicates the adopted categories and selected parameters for the rock samples as a representative of each category based on the RMR classification. RMR system represents an engineering classification of rock mass utilized to evaluate the quality of the rock with considering six parameters named uniaxial compressive strength (UCS), designation of rock quality (RQD, spacing of discontinuity, condition of discontinuity, conditions of groundwater; and orientation of discontinuity. The method is also used to estimate the tunnel stand-up time. Representative values were determined for a median sample of each category. Each rock mass group's parameters were calculated by RocLab software. The software inputs are the uniaxial compressive strength of intact rock, Geological strength index (GSI), rock disturbance factor, and constant value of rock mass (mi). The outputs are elastic modulus of the rock mass, shear strength parameters, and uniaxial compressive strength of rock mass. The calculated parameters for each rock group in numerical modeling are shown in Table 4.

Table 3. Suggested parameters range for rock categories

| Rock type | Sample | $\sigma_{ci}$ (MPa) | RMR | GSI | Mi |
|---|---|---|---|---|---|
| Strong | Conglomerates | 50-100 | 61-80 | 56-75 | 16-22 |
| Medium | Sandstone | 25-50 | 41-60 | 36-55 | 11-15 |
| Poor | Marl | 5-25 | 21-40 | 16-35 | 6-10 |
| Very poor | Shale | 1-5 | < 20 | 0-15 | 0-5 |

Table 4. Calculated parameters of each representative group of rocks for numerical modeling

| Rock type | Em (MPa) | $\sigma_{cm}$ (kPa) | Φ (deg.) | C (kPa) | Ψ (deg.) | GSI residual | C residual (kPa) |
|---|---|---|---|---|---|---|---|
| Strong | 15400 | 21382 | 38.60 | 3860 | 6.75 | 26.85 | 2288 |
| Medium | 3326 | 5352 | 29.09 | 1180 | 2.18 | 23.40 | 852 |
| Poor | 1060 | 1700 | 21.35 | 435 | 0 | 17.88 | 354 |
| Very poor | 300 | 228 | 14.95 | 65.65 | 0 | 12.27 | 58 |

## 5. Results and Discussions

### 5.1. The Vertical Settlements of the Tunnel Crown and the Invert Heave

Numerical analysis was used to obtain the tunnel crown settlements and invert heave along the longitudinal axis under various constitutive models for different types of rocks. Fig. 3 displays the vertical displacement contours for very weak rocks, while Fig. 4 compares the vertical displacement for each rock category.

For very weak rocks, the VM model predicts the highest crown settlement and invert heave at 24.5 mm and 22.5 mm, respectively, compared to other constitutive models. The MC, DP, and LE models have lower predictions with crown settlement values of 14.8, 10.8, and 8.7 mm and invert heave values of 17.6, 15.8, and 15.2 mm, respectively. In this rock group, the difference between the MC and DP models is significant, with MC predicting a higher value than DP, and the LE model predicting the lowest value. However, the FE equations of GHB, GHBR, and SS constitutive models did not converge in this rock group.

For weak, moderate, and strong rocks, the VM, DP, and MC models predict almost the same values for crown settlements and invert heaves, while the SS model provides higher values than other models. The SS model's

predictions for medium rocks are slightly different from other models, while for strong rocks, it is similar to other models' predictions.

Except for very weak rocks, both GHB and GHBR models predict higher values for crown settlements along the tunnel axis than other constitutive models. Furthermore, as the rock strength increases from weak to strong, the predicted values become closer to those of other constitutive models. The GHB model provides the highest value in the tunnel's invert heave for weak rocks, while GHBR has the lowest value. However, in moderate and strong rocks, GHBR has the highest, and the LE model has the lowest values in predicting the tunnel's invert heave.

## 5.2. Ground surface settlement induced by tunnel excavation

Figures 5 and 6 present the surface settlement longitudinal profile and cross-section for different constitutive models in the studied rocks. The measurements were taken at a cross-section located 18 m from the tunnel face, which is twice the tunnel diameter, or 36 m from the beginning of the model. The Panet equation (Sulem et al., 1987) was used to calculate the results. This location was selected because 98% of the total tunnel displacements are due to the advancing of the tunnel face at this distance, without the interference of the creep and time-dependent behavior of rocks (Asadollahpour et al., 2014).

Observations reveal that the ground surface settlement has a parabolic shape, and its vertex aligns with the tunnel's center. In Fig. 7, the maximum values of ground surface settlements are compared at a distance twice the tunnel's face diameter. Notably, as the rocks grow stronger, the differences in ground surface settlement values decrease. The GHBR constitutive model consistently predicts higher levels of ground surface settlement than other models.

Fig. 7(a) depicts that, for very weak rocks, the VM model predicts the highest maximum value of ground surface settlement, while the LE model predicts the lowest. Comparatively, the Mohr-Coulomb model produces higher values than the DP model. Moreover, as per Fig. 5(a), the LE, DP, and MC models suggest a slight heave on the ground surface when moving away from the cross-section's center for very weak rocks. The VM model shows a 1387% higher surface settlement than the LE model, while the MC model shows 508%, and the DP model shows 219% higher surface settlements.
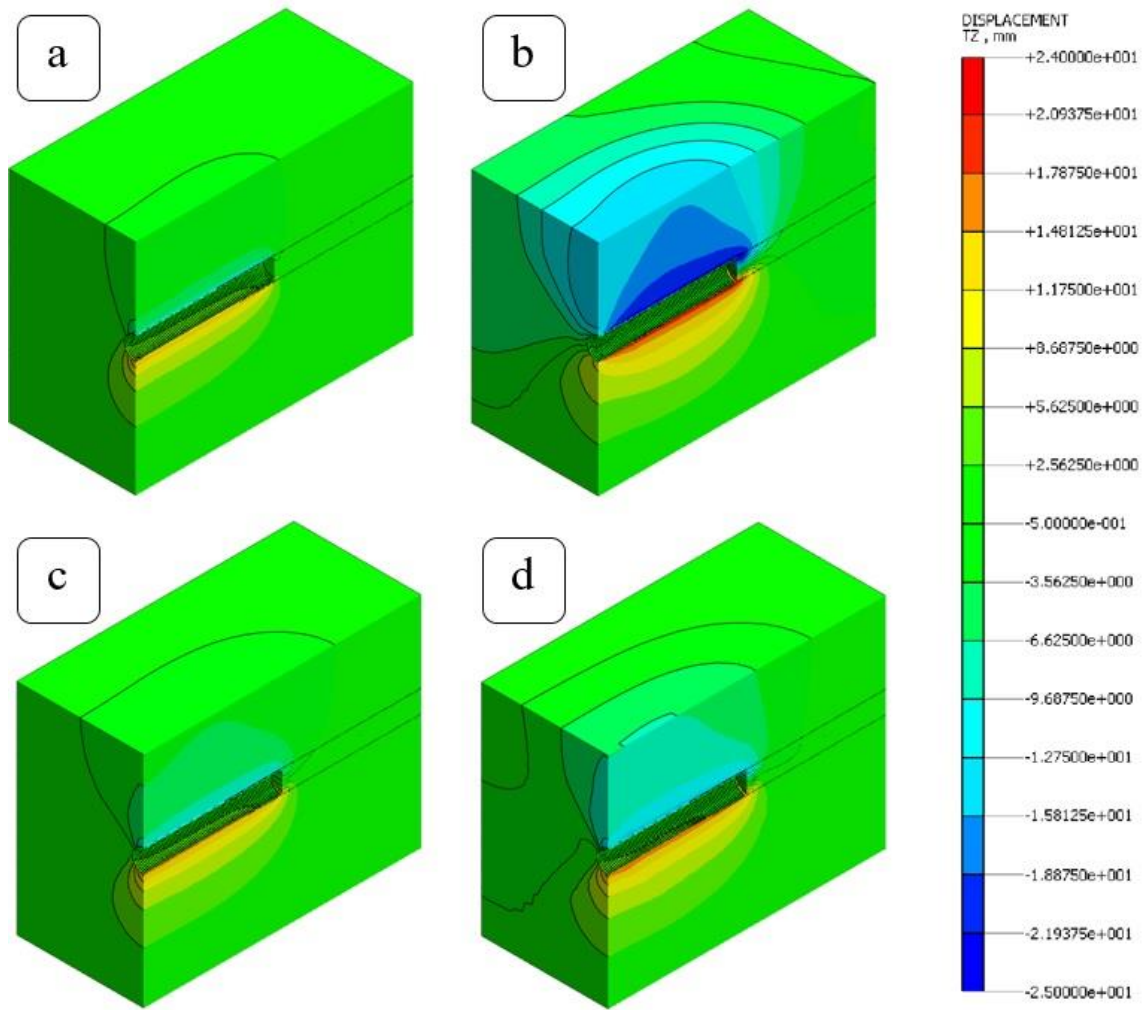
Fig. 3. Vertical displacement contours for a) LE, b) VM, c) DP, and d) MC models in very weak rock



(a)

(b)



(c)



(d)

12
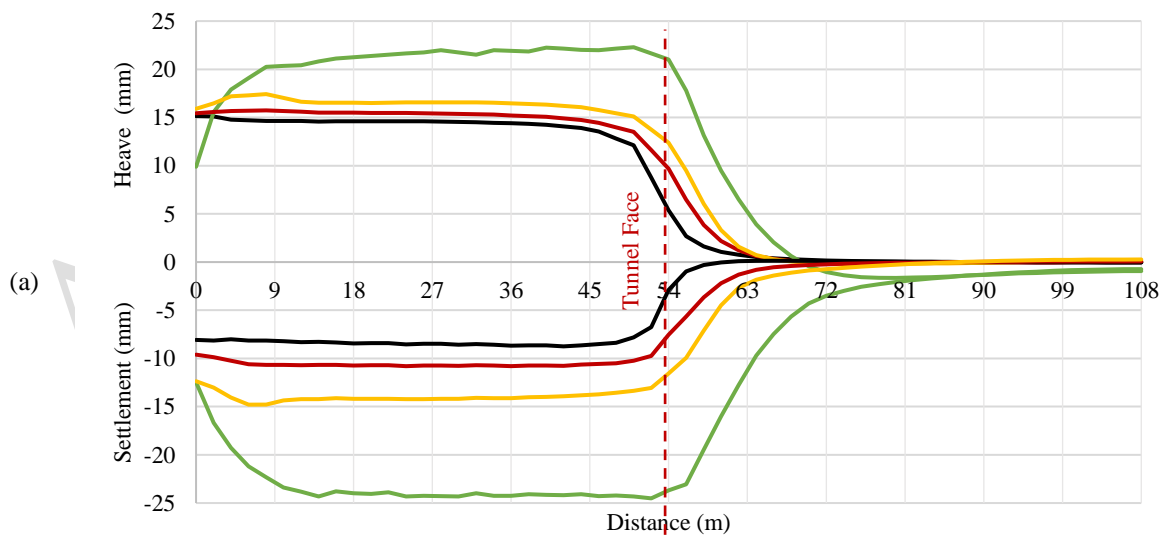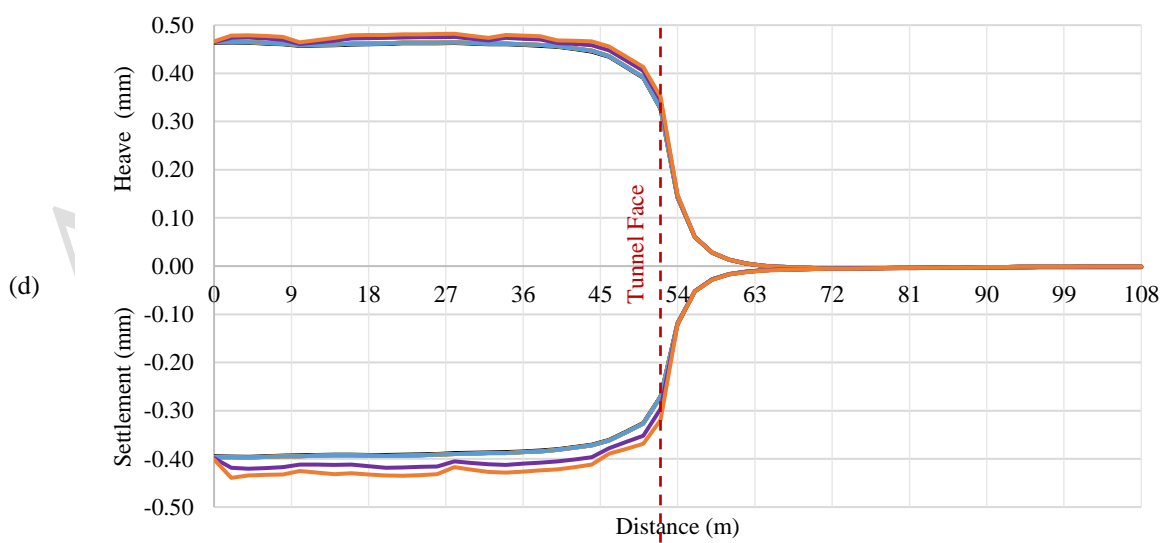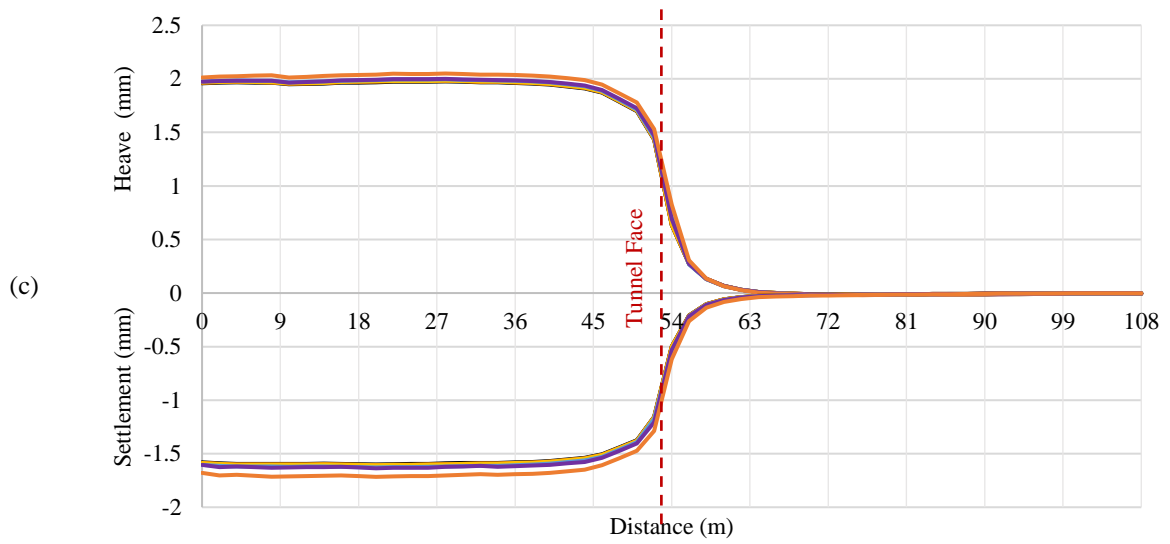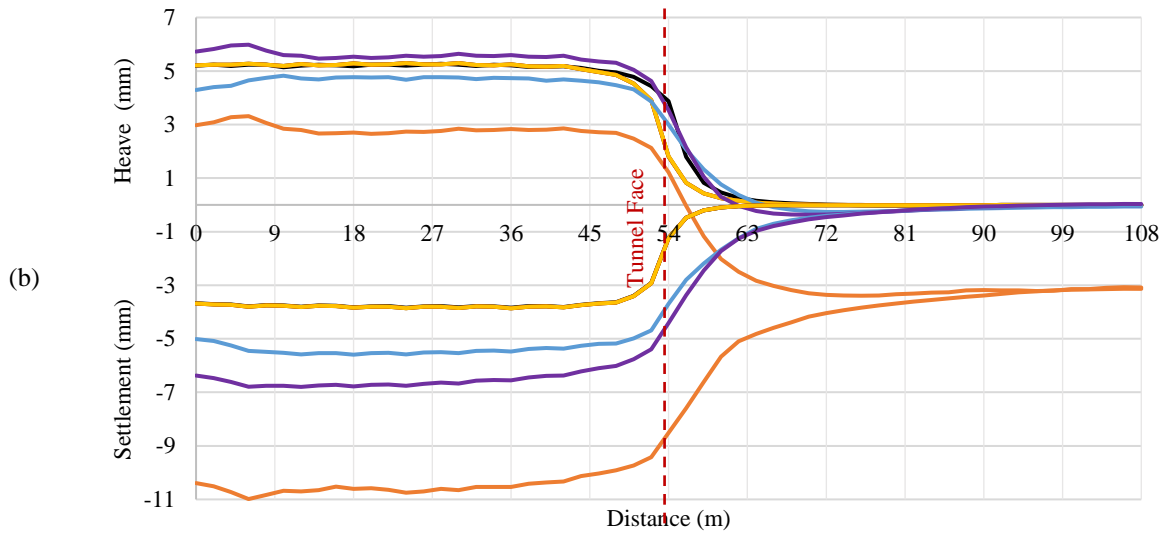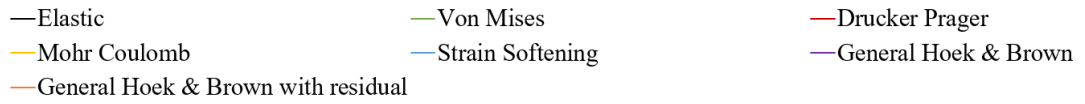
Fig. 4: Vertical settlements of the tunnel crown and the invert heave along the longitudinal axis of the tunnel for a) very weak, b) weak, c) moderate, and d) strong rocks

(d)

Legend:
- ----- Drucker Prager
- —·- Generalized Hoeak & Brown
- --- Mohr Coulomb
- ········ Von Mises
- —— Elastic
- —··- Generalized Hoeak & Brown with residual parameters
- — — Strain softening
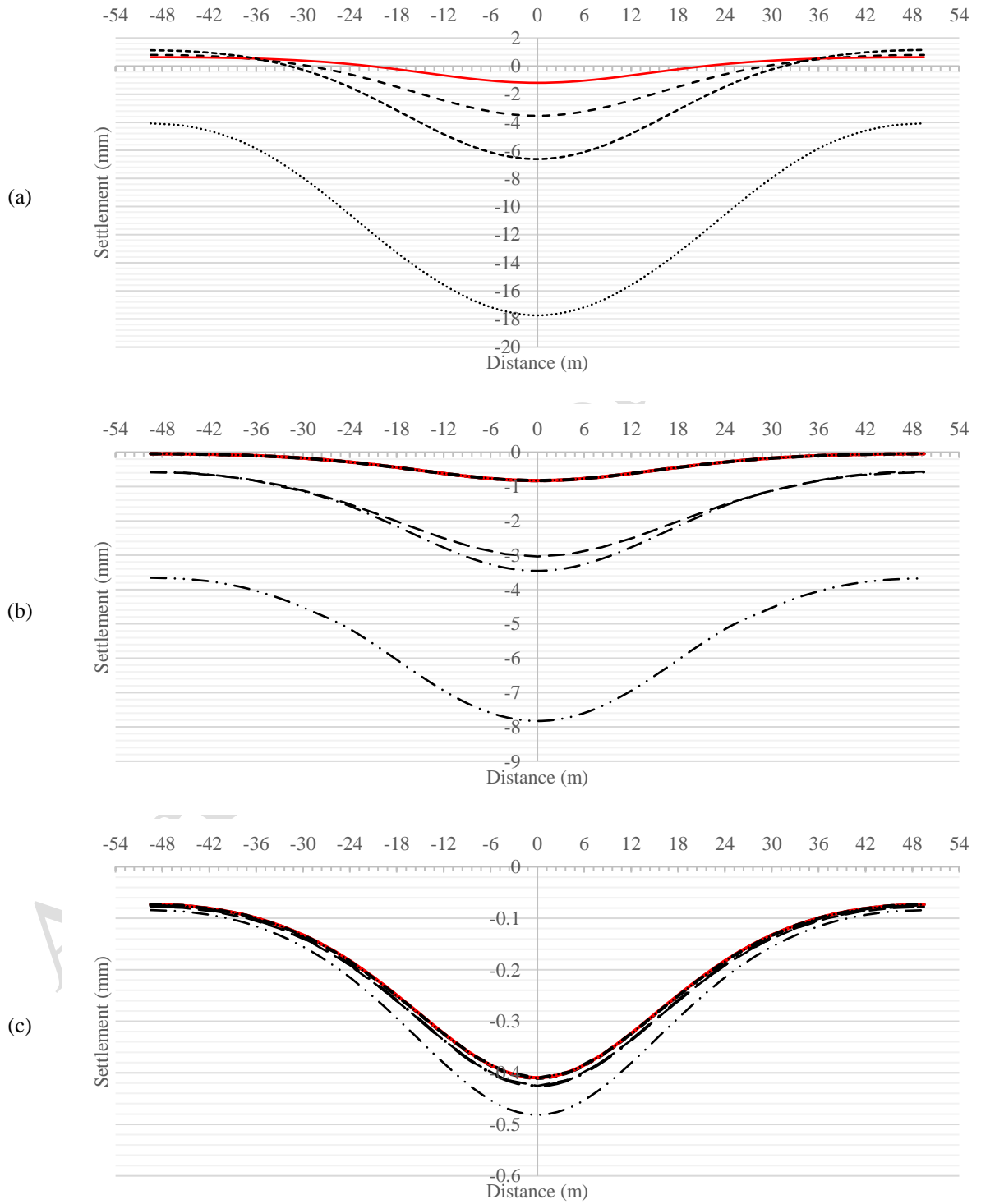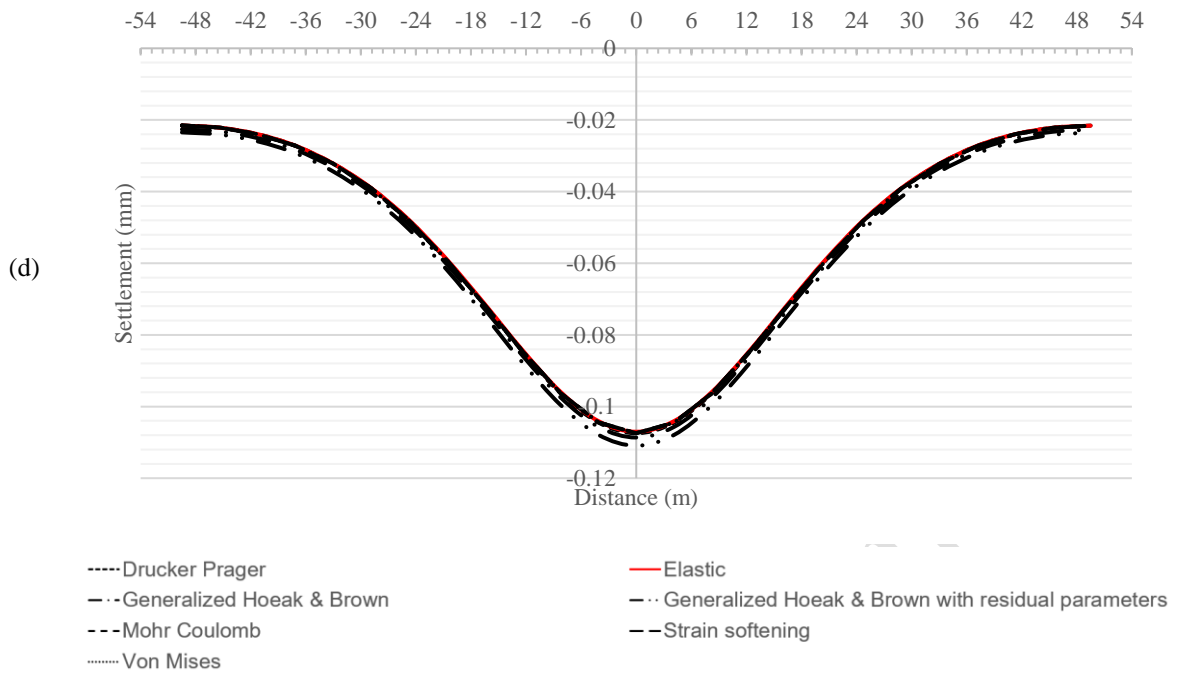
Fig. 5. Surface settlement cross-section for a) very weak, b) weak, c) moderate, and d) strong rocks



(a)



(b)

14

(c)



(d)

Legend:
- Elastic (red solid line)
- Von Mises (dotted line)
- Drucker Prager (dashed line)
- Mohr Coulomb (dashed line)
- Strain softening (long dash line)
- Generalized Hoek & Brown (dash-dot line)
- Generalized Hoek & Brown with residual parameter (dash-dot-dot line)
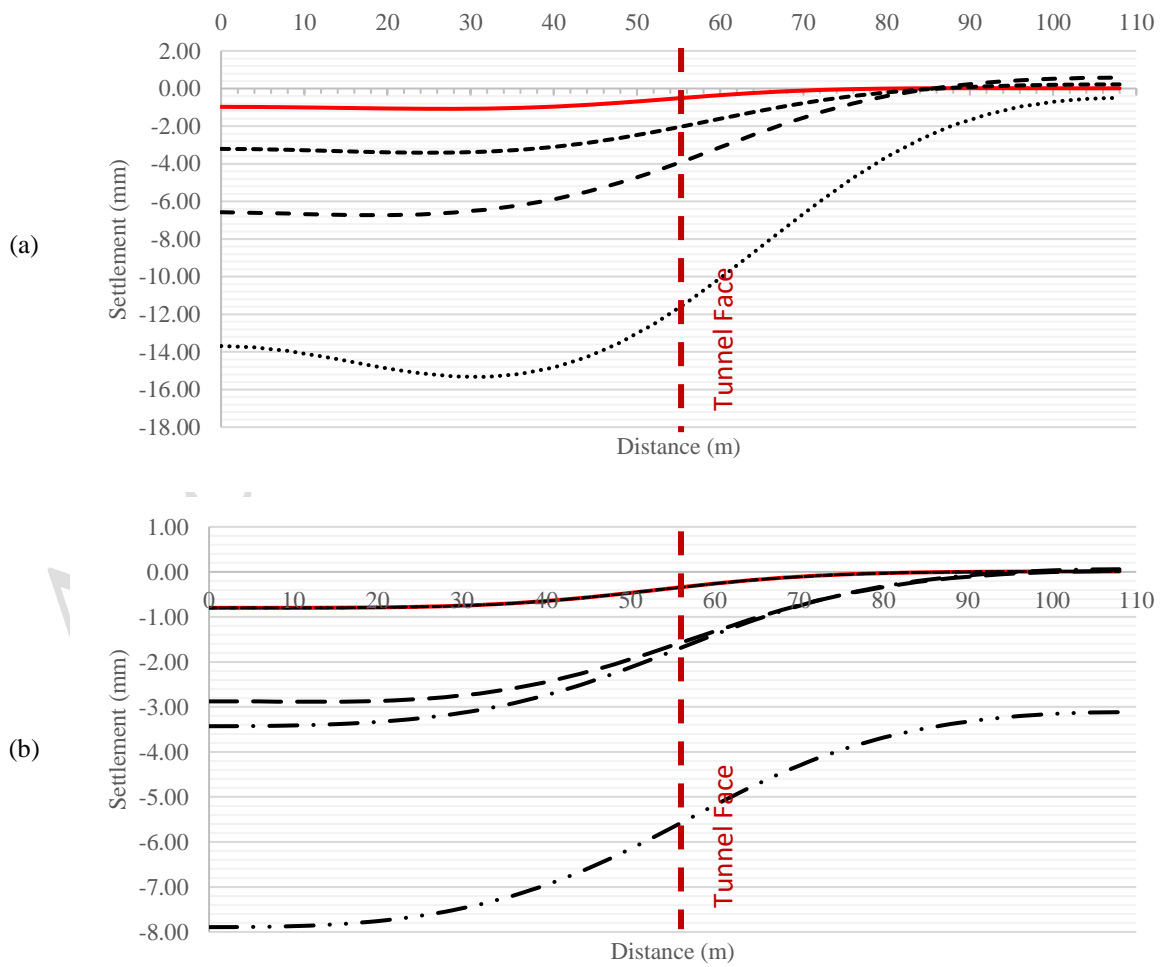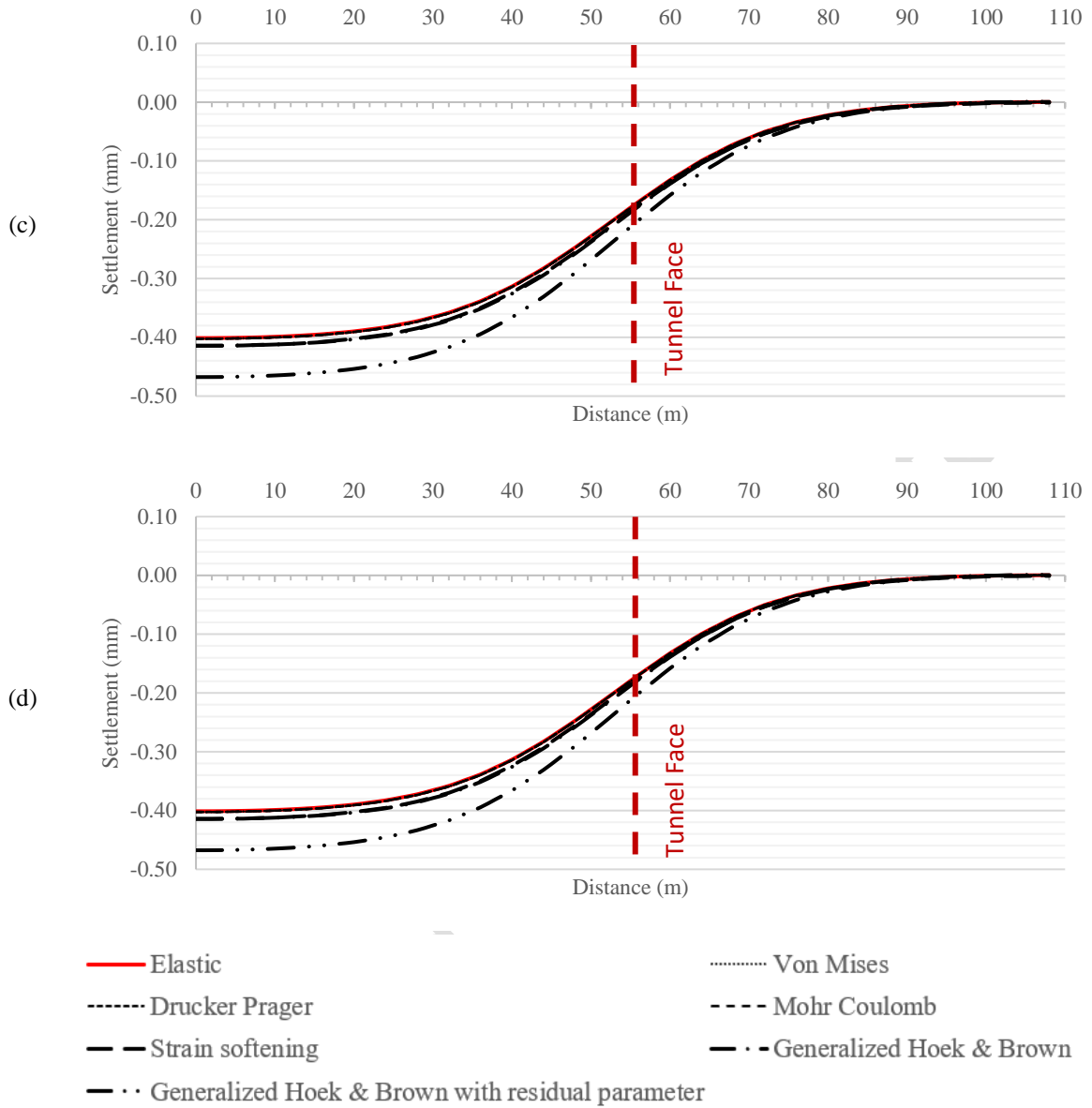
Fig. 6. Longitudinal profile of surface settlement for a) very weak, b) weak, c) moderate, and d) strong rocks

(a)



| | MC | DP | VM | EL | Ave. |
|---|---|---|---|---|---|
| Very weak | 6.2 | 3.25 | 15.17 | 1.02 | 6.41 |

15
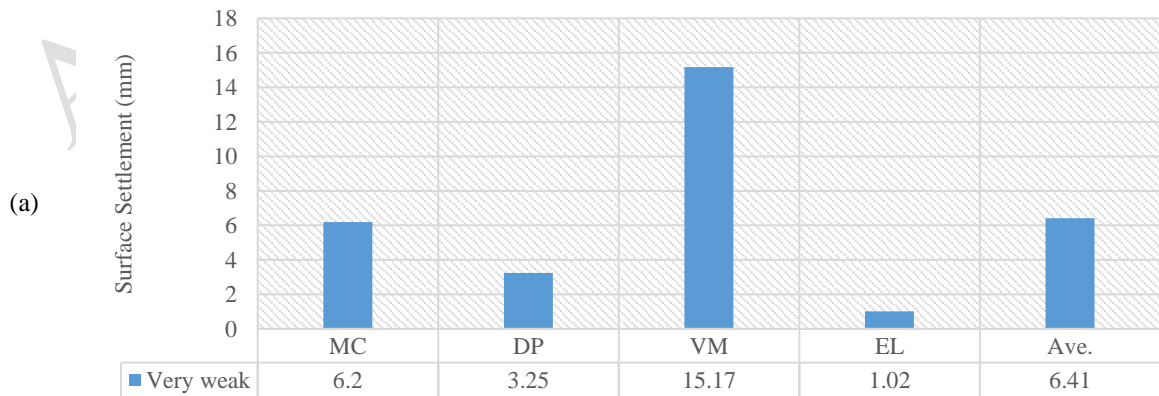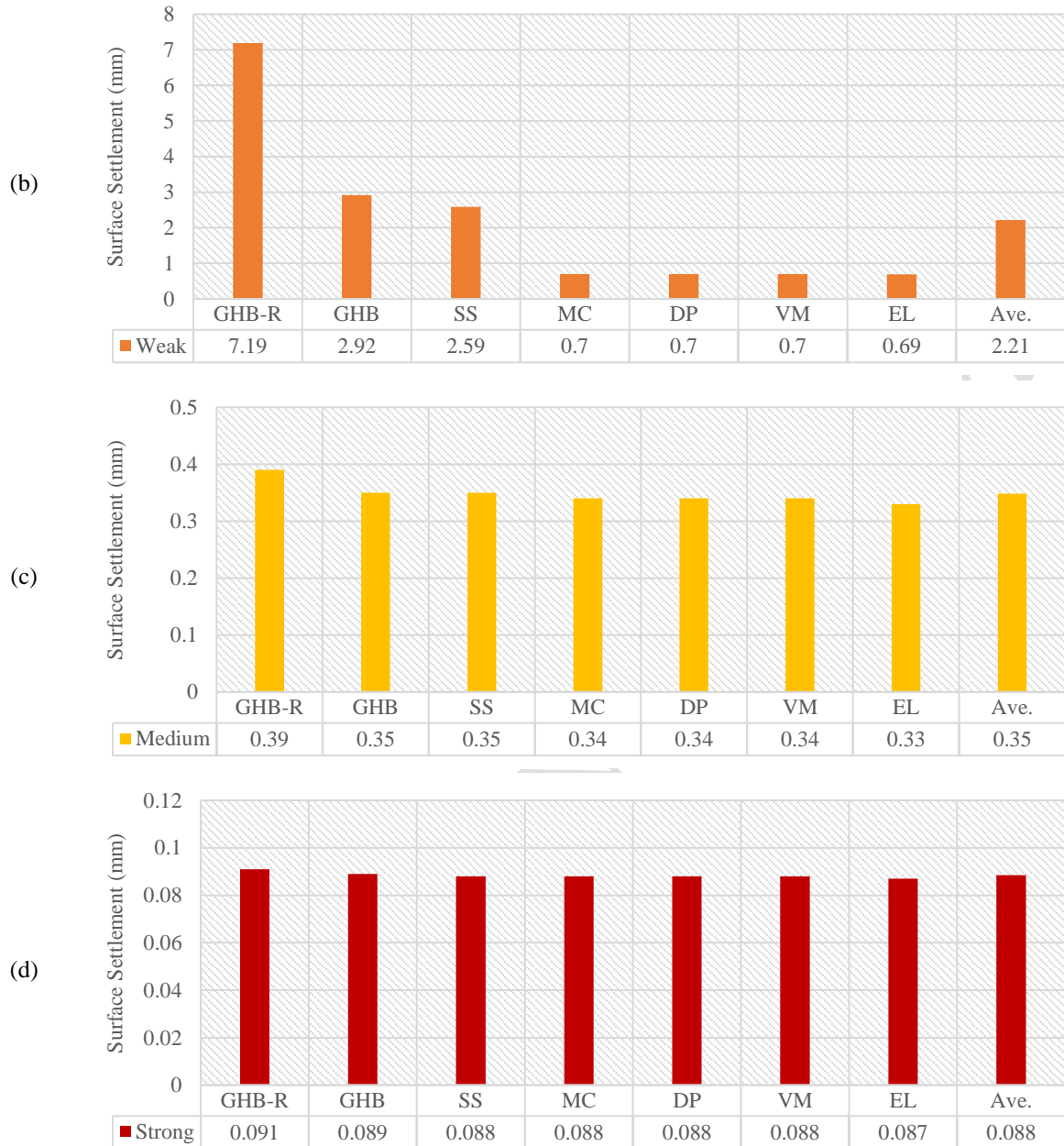
Fig. 7. Maximum surface settlements of the cross-section for a) very weak, b) weak, c) moderate, and d) strong rocks

In the weak rock category, as shown in Fig. 5(b), the settlement value reaches zero by moving away from the center of the cross-section. The GHBR model has predicted the maximum value of the ground surface settlement, followed by the GHB and then the SS constitutive models showing the second and third highest values. According to Fig. 5(b), the difference between SS and GHB constitutive models is in their ground surface settlement curves' vertex values. The two curves will coincide by moving away from the center of the cross-section to the sides. Fig. 7(b) indicates that the VM, DP, and MC models offer the same results, and the LE model has a slightly lower value. The difference is only 1.45%, which is inconsiderable. However, the maximum values of the ground surface settlement in SS, GHB, and GHBR are 275, 323, and 942%, respectively, more than the LE model.

Regarding the results shown in Fig. 7(c), for medium rocks, the differences between the predicted values of ground surface settlement by each constitutive model have been reduced. It is evident that in this category of rocks, the predicted values of GHBR are greater than other constitutive models. By comparing the maximum

16

ground surface settlement of each constitutive model with the LE model, it was observed that VM, DP, and MC, indicate 3% greater value, SS and GHB models show a 6.1% greater value, and GHBR shows a value that is 18.2% greater than the maximum surface settlement predicted by LE model.

In the strong rocks, according to the results shown in Fig. 7(d), compared to the LE constitutive model, VM, DP, MC, and SS models show a value of 1.15%, GHB shows a value that is 2.3%. GHBR offers a value that is 4.6% greater than the ground surface settlement of the LE model. The minor differences between the results obtained from all the constitutive models for moderate and strong rocks compared to the LE model's values indicate that all these models can reasonably predict the elastic behavior of these rock categories.

## 5.3. Stresses applied to the support system

Fig. 8 shows the Z-Z vertical stress contours for very weak rocks, in the concrete segment, at a distance of twice the diameter of the tunnel face. In Figs. 9(a)-(b), the Z-Z and Z-X's maximum vertical and shear stresses are shown, respectively. In general, in all the constitutive models, when the rocks get stronger, the maximum stress values applied to the support system have decreased as well as the difference in the calculated stresses by each constitutive model.

The LE constitutive model shows the highest value in the Z-Z direction for the very weak rock category. Afterward, MC and DP have the same results, and then the VM model has the lowest value.

In the weak rocks, according to Fig. 9(a), among the studied constitutive models, the maximum vertical stress is predicted by SS model, then GHB and GHBR models, and then, the three constitutive models of MC, DP, and VM, and eventually the LE model.
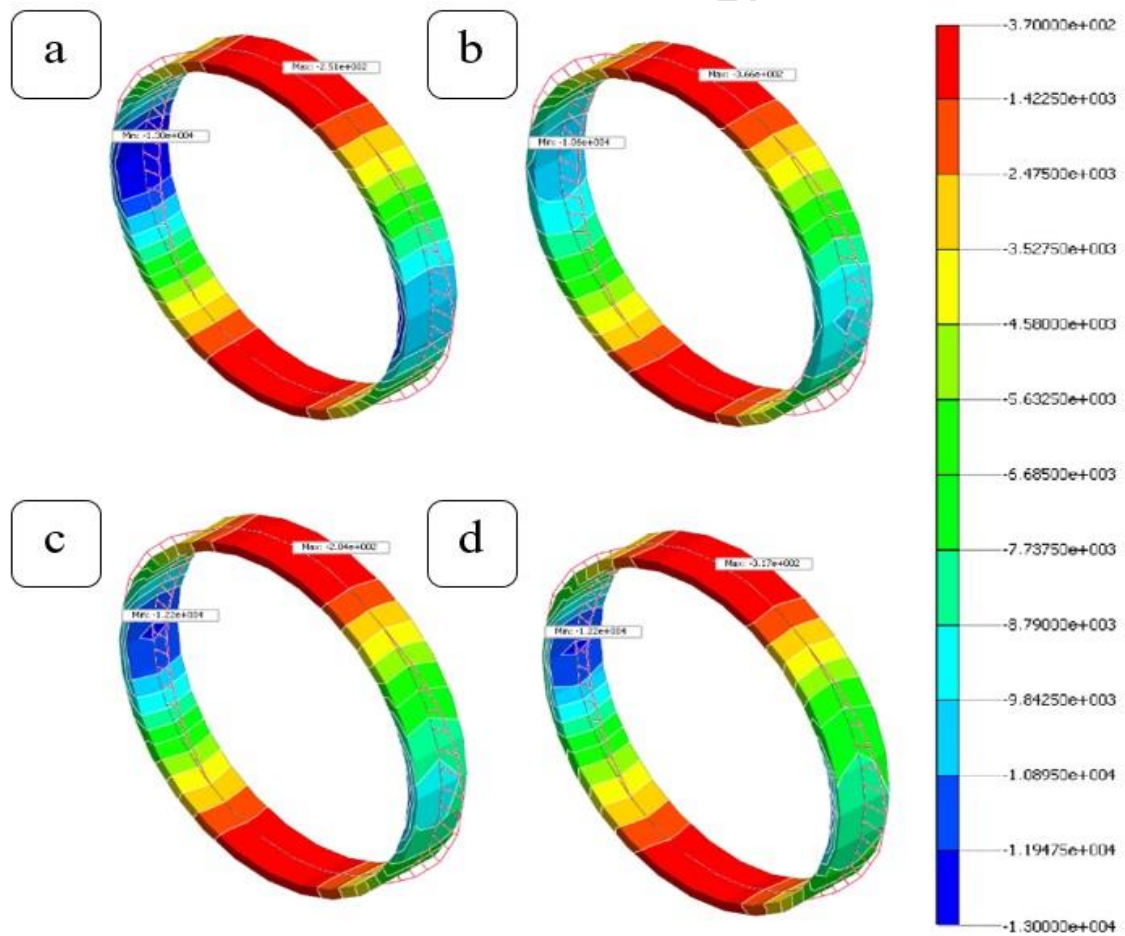


Fig. 8. Vertical stress contours for a) LE, b) VM, c) DP, and d) MC models in very weak rock

a)

17

## Stress Z-Z (kN/m2)



| | Generalized Hoek & Brown with residual | Generalized Hoek & Brown | Mohr Coulomb | Druker Prager | Strain Softening | Von Mises | Elastic |
|---|---|---|---|---|---|---|---|
| ■ S Z-Z Very Weak | | | 1.24E+04 | 1.22E+04 | | 1.10E+04 | 1.30E+04 |
| ■ S Z-Z Weak | 9.54E+03 | 9.19E+03 | 8.11E+03 | 8.10E+03 | 9.84E+03 | 8.10E+03 | 8.08E+03 |
| ■ S Z-Z Medium | 4.64E+03 | 4.05E+03 | 3.75E+03 | 3.75E+03 | 4.20E+03 | 3.75E+03 | 3.72E+03 |
| ■ S Z-Z Strong | 1.09E+03 | 1.05E+03 | 1.05E+03 | 1.05E+03 | 1.05E+03 | 1.05E+03 | 1.03E+03 |

b)

## Stress Z-X (kN/m2)



| | Generalized Hoek & Brown with residual | Generalized Hoek & Brown | Mohr Coulomb | Druker Prager | Strain Softening | Von Mises | Elastic |
|---|---|---|---|---|---|---|---|
| ■ S Z-X Very Weak | | | 4.50E+03 | 4.46E+03 | | 5.48E+03 | 4.97E+03 |
| ■ S Z-X Weak | 3.52E+03 | 3.37E+03 | 3.07E+03 | 3.07E+03 | 4.00E+03 | 3.07E+03 | 3.06E+03 |
| ■ S Z-X Medium | 1.77E+03 | 1.49E+03 | 1.42E+03 | 1.42E+03 | 1.47E+03 | 1.42E+03 | 1.41E+03 |
| ■ S Z-X Strong | 5.81E+02 | 5.69E+02 | 5.53E+02 | 5.53E+02 | 5.53E+02 | 5.53E+02 | 5.52E+02 |

Fig. 9. Absolute Maximum stresses in a) Z-Z, and b) Z-X direction

The GHBR model has the highest stress in the Z-Z direction in the medium rocks. This is followed by the SS model and GHB, having the exact predictions, then the three constitutive models of MC, DP, and VM, and the lowest value of stress belongs to the LE model.

In the strong rock category, the result of Z-Z stress from highest to lowest is attributed to GHBR, having the highest stress value prediction, then, the four constitutive models of SS, MC, DP, and VM with the same values, then, the GHB, and finally the LE model.

Since the linear elastic constitutive model does not have a failure limit, it cannot predict the failure phenomenon. Therefore, in the range of very weak rocks, the LE model, in the assumed conditions for the tunnel, shows the stress values in the Z-Z direction more than other constitutive models, because in the other models, when reaching the yield status, the yielded FEs will no longer stand additional stress. In weak to strong rocks, due to characteristics of the examined tunnel, owing to the resistance of the rock, the failure did not occur, and therefore the elastic model does not have the highest stress value.

According to the results of Fig. 9(b), the VM constitutive model shows the maximum stress value in the Z-X direction for the very weak rocks. After that, the LE and MC models have a lower value than the VM model, and finally, the lowest value belongs to DP.

The GHBR and SS have similar results in the weak rock category, with the maximum shear stress value in the Z-X direction. Afterwards, the three constitutive MC, DP, and VM models provide the same results. The minimum value is predicted using the LE model.

In the medium rocks, the highest value of shear stress in the Z-X direction is attributed to GHBR. Subsequently, the GHB and SS models have the same value, lower than the GHB value. The next are the three constitutive models of MC, DP, and VM. Finally, similar to the behavior of weak rocks, the LE model predicts the minimum value.

In the strong rock category, the maximum stress in the Z-X direction is shown by the GHBR and then the GHB, and after these two models, SS, MC, DP, and VM models have the same results. The lowest value belongs to simulations with the LE model.

## 6. Parametric Analysis

The following section presents parametric studies based on the LE, MC, and GHB models for three sensitive parameters in numerical modeling: specific gravity, Poisson's ratio, and dilation angle. Weak rock category was adopted as a representative to perform the parametric analysis.

### 6.1. Specific Gravity

As shown in Fig. 10, specific gravity is changed in the range of 21-27 $kN/m^3$ . The ground surface settlement cross-section has been drawn for the LE, MC, and GHB models.
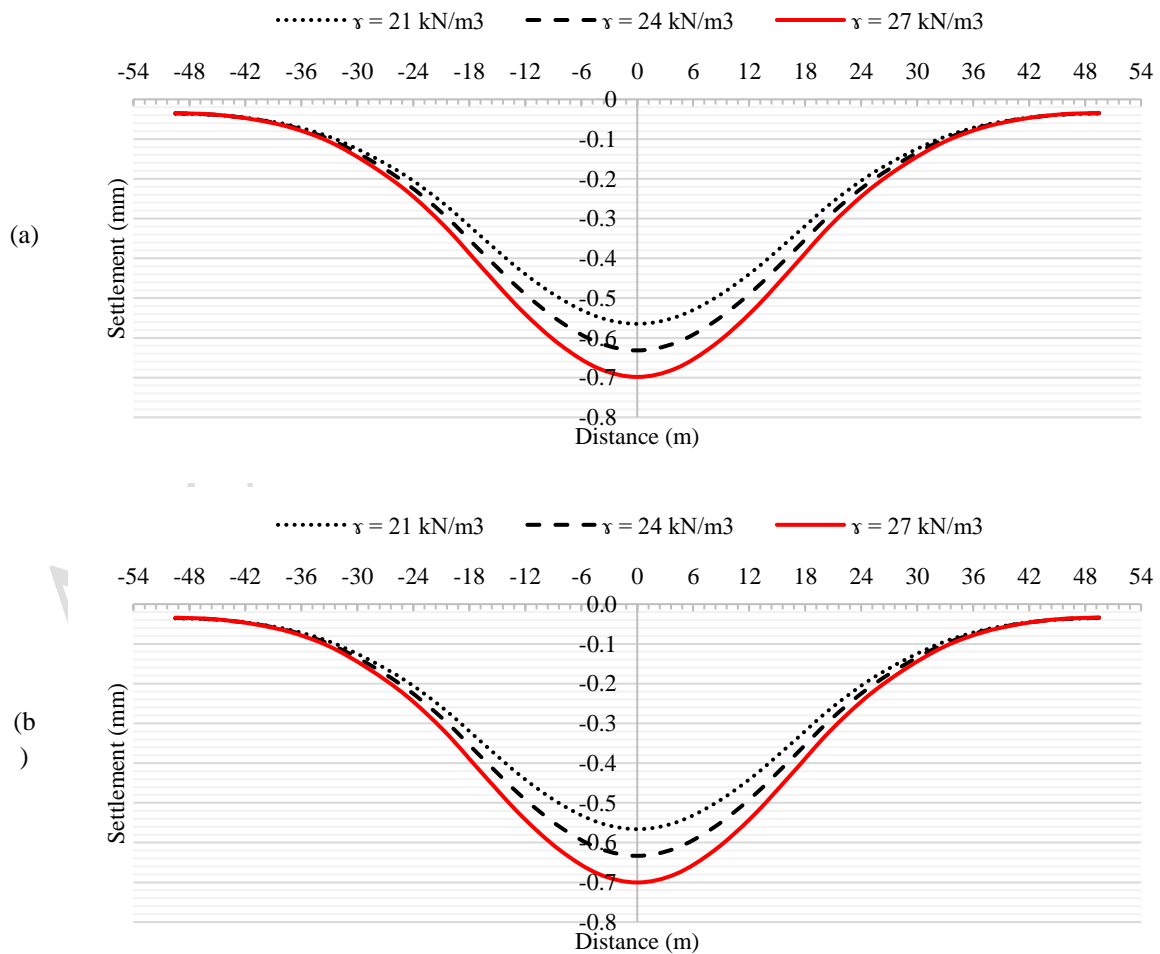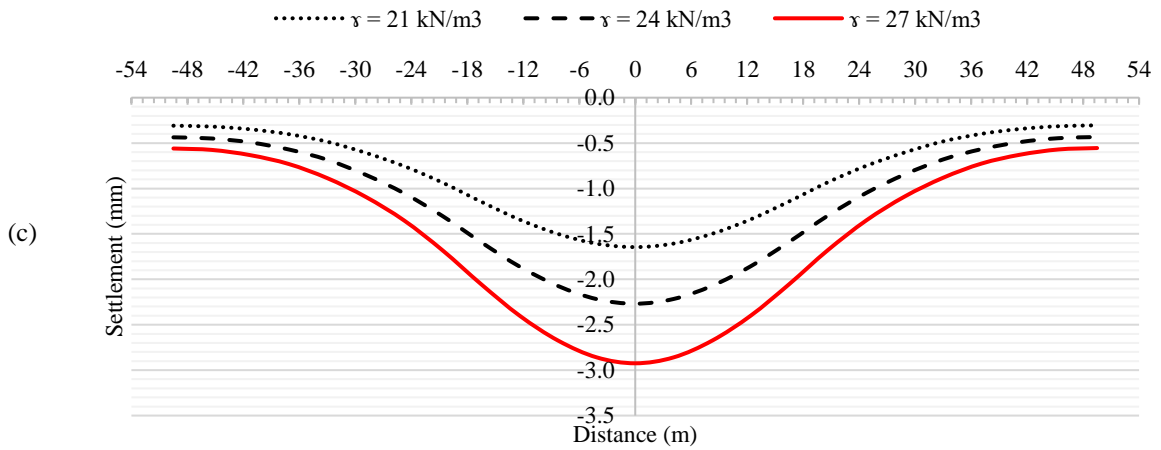
Fig. 10. Ground surface settlements in parametric analysis on specific gravity for a) LE, b) MC, and c) GHB models

It is evident that decreasing the specific gravity in all models results in a reduction of the maximum ground surface settlement. The greatest decrease is observed in the GHB model, while the lowest is seen in the LE model. Additionally, the changes in the broader area of cross-section are more widespread in the GHB model. Specifically, a reduction of three $^{kN}/_{m^3}$ in specific gravity, from 27 to 24 $^{kN}/_{m^3}$, results in a 29% drop in maximum settlement for the GHB model, as well as 10.6% for MC and 10.58% for the LE model. Similarly, a reduction of specific gravity from 24 to 21 kN∕m^3 leads to a 38%, 11.85%, and 11.83% decrease in maximum settlement for the GHB, MC, and LE models, respectively.

## 6.2. Poisson's Ratio

In Fig. 11, Poisson's ratio of the rock is changed in the range of 0.2-0.4, and the ground surface settlement cross-section has been shown for the LE, MC, and GHB constitutive models.
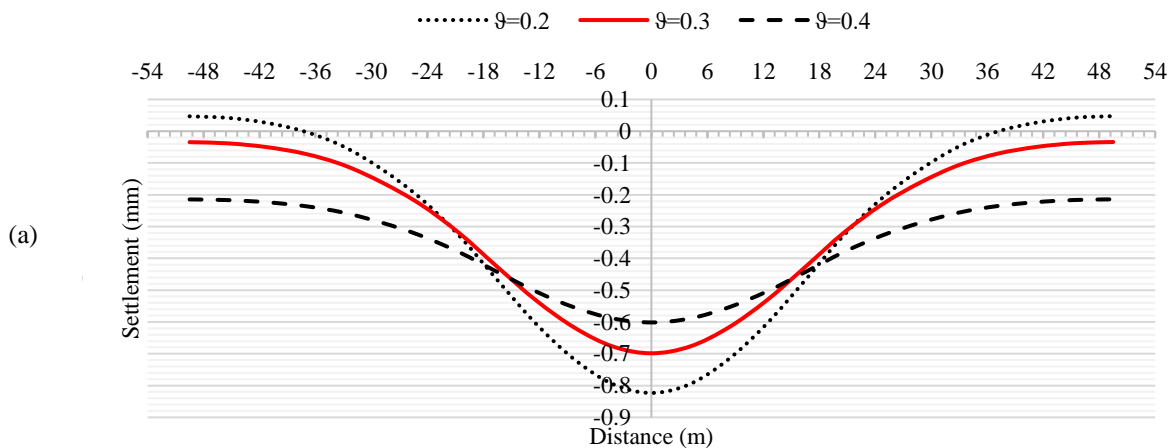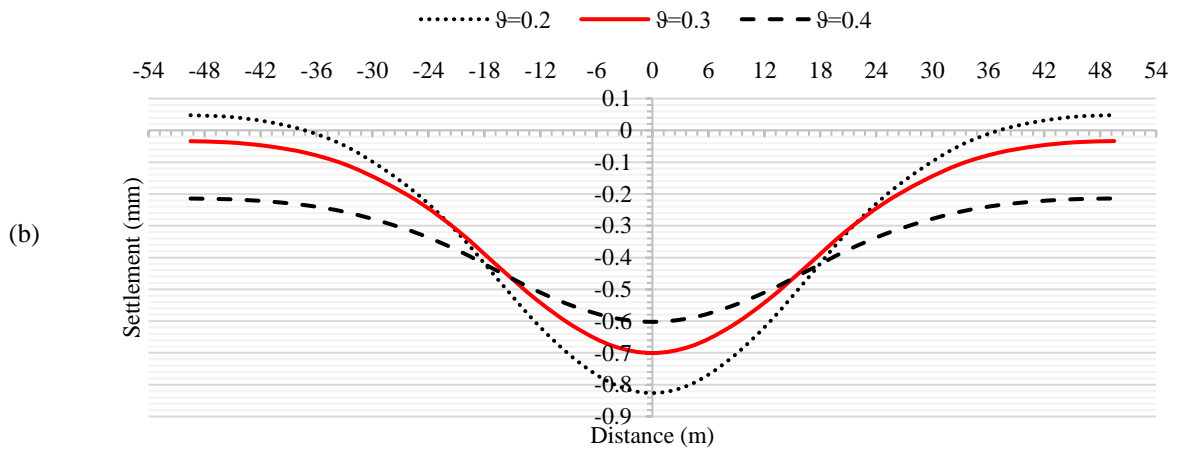
Fig. 11. Ground surface settlements in parametric analysis on Poisson's ratio for a) LE, b) MC, and c) GHB models

As demonstrated by all the models, increasing the Poisson's ratio results in a decrease in the maximum ground surface settlement. The GHB model exhibits the highest magnitude of decrease, while the LE model displays the lowest. Additionally, in the MC and LE models, decreasing the Poisson's ratio results in a tighter parabola for the cross-section of ground surface settlements, with settlements decreasing away from the center of the parabola. When the Poisson's ratio equals 0.2, ground surface heave can be observed. Increasing the Poisson's ratio from 0.2 to 0.3 leads to a 58.6% drop in maximum settlement for GHB, 18% for MC, and 17.85% for the LE model. Similarly, increasing the Poisson's ratio from 0.3 to 0.4 results in a 210%, 16.3%, and 16.12% decrease in maximum settlement for GHB, MC, and LE, respectively.

## 6.3. Dilation Angle

As illustrated in Figure 12, the rock's dilation angle has been varied between 0 and 5 degrees, and the ground surface settlement cross-section has been plotted for the MC and GHB constitutive models. It is worth noting that the LE model does not account for the dilation angle.

As depicted in the figure, an increase in the GHB model's dilation angle results in a decrease in the maximum settlement of the ground surface. Specifically, each 2.5-degree increase in the dilation angle leads to a 7% reduction in the maximum cross-section settlement. Conversely, changing the dilation angle does not have an impact on the ground surface settlement results for the MC model.
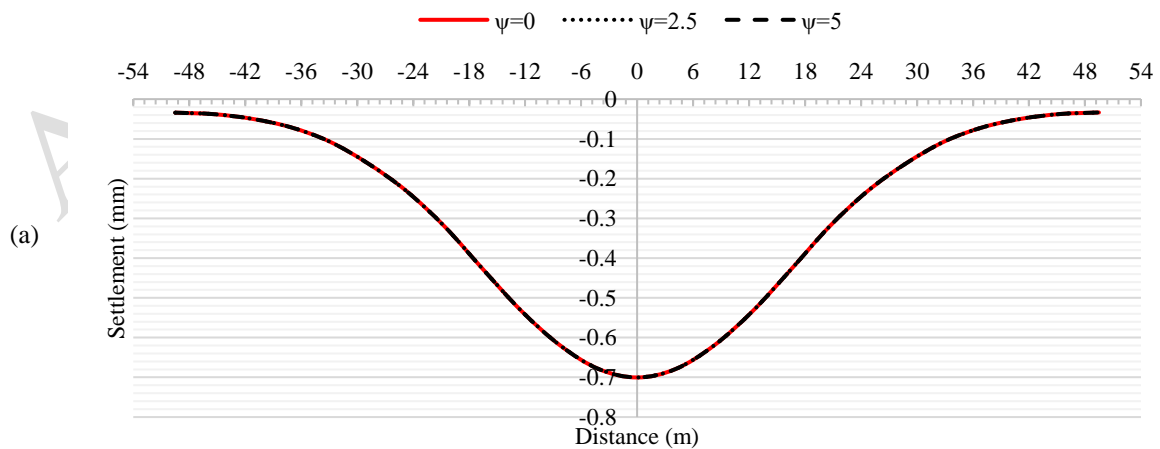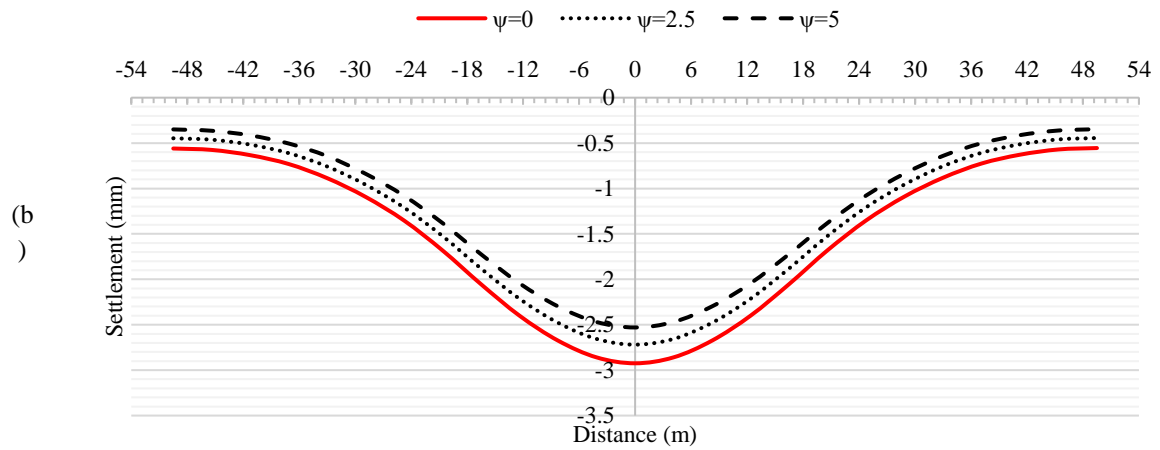
Fig. 12. Ground surface settlements in parametric analysis on dilation angle for a) MC, and b) GHB models

## 7. Conclusions

In this study, numerical modeling was employed to evaluate the behavior of tunnels under different constitutive model. A series of 3D finite element simulations were conducted to investigate the impact of various constitutive models and associated parametric analyses on tunnel behavior during typical rock medium construction with varying strengths. The simulations focused on analyzing displacements, ground surface settlements, and support system stresses across seven models. Furthermore, parametric analyses were performed on specific gravity, Poisson's ratio, and the rock's dilation angle for the LE, MC, and GHB constitutive models. Based on the analyses conducted, the following results can be presented for the prediction of rock tunnel behavior using the aforementioned models under the assumed conditions of this study:

- Constitutive models play a crucial role in numerical modeling as they represent material behavior and significantly impact analysis results. Therefore, selecting an appropriate model based on accurate data is essential to predict results accurately.

- It is important to note that the LE constitutive model lacks a failure criterion, making it unsuitable for situations where element failure is likely. This model tends to underestimate deformations and overestimate stresses in very weak rocks. However, it can be used for a first estimation of deformations in strong rocks since it requires less modeling time than other models.

- Some constitutive models more accurately predict displacements and induced lining stresses in the specific strength rock category. Therefore, the appropriate model should be selected by considering the existing mechanical parameters and the rock's strength range.

- Rock-specific constitutive models such as GHB and GHBR are more sensitive to parameter variations than soil-established models like MC and DP. General models like LE and VM are less sensitive.

- In the parametric analysis of specific gravity, increasing this parameter increases ground surface settlements and stresses on the tunnel support system. Therefore, determining the rock's specific gravity accurately is recommended for design purposes.

- A small increase in Poisson's ratio can significantly reduce tunnel and ground surface settlements. Thus, accurately testing rock samples and considering the correct Poisson's ratio for the material can be very effective in the design.

- For the GHB constitutive model, increasing the medium's dilation angle in the range of weak rocks will decrease tunnel and ground surface settlements. However, this parameter's increase in strong rocks will not significantly affect the results. The MC constitutive model results are not affected by changes in the dilation angle within the range of assumptions made.

22

# References

Aksoy, C. O., & Uyar, G. G. (2017). Non-deformable support system in swelling and squeezing rocks. Rock Mechanics and Engineering, 4, 179-203.

Anato, N. J., Chen, J., Tang, A., & Assogba, O. C. (2021). Numerical investigation of ground settlements induced by the construction of Nanjing WeiSanLu tunnel and parametric analysis. Arabian Journal for Science and Engineering, 46(11), 11223-11239. https://doi.org/10.1007/s13369-021-05642-3

Asadollahpour, E., Rahmannejad, R., Asghari, A., & Abdollahipour, A. (2014). Back analysis of closure parameters of Panet equation and Burger′s model of Babolak water tunnel conveyance. International Journal of Rock Mechanics and Mining Sciences, 68, 159-166. https://doi.org/10.1016/j.ijrmms.2014.02.017.

Audi, Y., Jullien, A., Dauvergne, M., Feraille, A., & Schwartzentruber, L. D. A. (2020). Methodology and application for the environmental assessment of underground multimodal tunnels. Transportation Geotechnics, 24, 100389. https://doi.org/10.1016/j.trgeo.2020.100389

Bakker, K. J. (2003). Structural design of linings for bored tunnels in soft ground. Heron, 48(1), 33-64.

Beyabanaki, A. R., & Gall, V. (2017). 3D numerical parametric study of the influence of open-pit mining sequence on existing tunnels. International Journal of Mining Science and Technology, 27(3), 459-466. https://doi.org/10.1016/j.ijmst.2017.03.018.

Bobet, A. (2001). Analytical solutions for shallow tunnels in saturated ground. Journal of engineering mechanics, 127(12), 1258-1266. https://doi.org/10.1061/(ASCE)0733-9399(2001)127:12(1258).

Cai, M., Kaiser, P. K., Tasaka, Y., & Minami, M. (2007). Determination of residual strength parameters of jointed rock masses using the GSI system. International Journal of Rock Mechanics and Mining Sciences, 44(2), 247-265. https://doi.org/10.1016/j.ijrmms.2006.07.005.

Carranza-Torres, C., Rysdahl, B., & Kasim, M. (2013). On the elastic analysis of a circular lined tunnel considering the delayed installation of the support. International Journal of Rock Mechanics and Mining Sciences, 61, 57-85. https://doi.org/10.1016/j.ijrmms.2013.01.010.

Chalajour, S., & Hataf, N. (2022). The Comparison of Tunnel Convergence from Numerical Analysis with Monitoring Data Based on Different Constitutive Models in Rock Medium. Civil Engineering Infrastructures Journal. https://doi.org/10.22059/CEIJ.2022.343391.1843

Chen, S. L., & Lee, S. C. (2020). An investigation on tunnel deformation behavior of expressway tunnels. Geomechanics and Engineering, 21(2), 215-226. https://doi.org/10.12989/gae.2020.21.2.215.

Davis, R. O., & Selvadurai, A. P. (2005). Plasticity and geomechanics. Cambridge university press.

Ding, L., & Liu, Y. (2018). Study on deformation law of surrounding rock of super long and deep buried sandstone tunnel. Geomechanics & engineering, 16(1), 97-104. https://doi.org/10.12989/gae.2018.16.1.097.

Goodman, R. E. (1989). Introduction to rock mechanics (Vol. 2, pp. 221-388). New York: Wiley.

He, M., Zhang, Z., Zheng, J., Chen, F., & Li, N. (2020). A new perspective on the constant mi of the Hoek–Brown failure criterion and a new model for determining the residual strength of rock. Rock Mechanics and Rock Engineering, 53, 3953-3967. https://doi.org/10.1007/s00603-020-02164-6

Hejazi, Y., Dias, D., & Kastner, R. (2008). Impact of constitutive models on the numerical analysis of underground constructions. Acta Geotechnica, 3, 251-258. https://doi.org/10.1007/s11440-008-0056-1.

Hoek, E., & Brown, E. T. (1997). Practical estimates of rock mass strength. International journal of rock mechanics and mining sciences, 34(8), 1165-1186. https://doi.org/10.1016/S1365-1609(97)80069-X

Hoek, E., & Brown, E. T. (2019). The Hoek–Brown failure criterion and GSI–2018 edition. Journal of Rock Mechanics and Geotechnical Engineering, 11(3), 445-463. https://doi.org/10.1016/j.jrmge.2018.08.001

Hoek, E., Wood, D., & Shah, S. (1992). A modified Hoek–Brown failure criterion for jointed rock masses. In Rock Characterization: ISRM Symposium, Eurock'92, Chester, UK, 14–17 September 1992 (pp. 209-214). Thomas Telford Publishing.

Hoek, E., Kaiser, P. K., & Bawden, W. F. (1995). Support of underground excavation in hard rock: Rotterdam. AA Balkema, 84-97.

Jallow, A., Ou, C. Y., & Lim, A. (2019). Three-dimensional numerical study of long-term settlement induced in shield tunneling. Tunnelling and Underground Space Technology, 88, 221-236. https://doi.org/10.1016/j.tust.2019.02.021.

Jin, Y. F., Zhu, B. Q., Yin, Z. Y., & Zhang, D. M. (2019). Three-dimensional numerical analysis of the interaction of two crossing tunnels in soft clay. Underground Space, 4(4), 310-327. https://doi.org/10.1016/j.undsp.2019.04.002

Lazemi, H. A., & Soleiman Dehkordi, M. (2019). Estimation of the TBM penetration rate using the post-failure behavior of a rock mass and the equivalent thrust per cutter. A case study: the Amirkabir Water Transferring Tunnel of Iran. Bulletin of Engineering Geology and the Environment, 78(3), 1735-1746. https://doi.org/10.1007/s10064-017-1205-2.

Li, C., Hou, S., Liu, Y., Qin, P., Jin, F., & Yang, Q. (2020). Analysis on the crown convergence deformation of surrounding rock for double-shield TBM tunnel based on advance borehole monitoring and inversion analysis. Tunnelling and Underground Space Technology, 103, 103513. https://doi.org/10.1016/j.tust.2020.103513

Li, G., Ma, F., Liu, G., Zhao, H., & Guo, J. (2019). A strain-softening constitutive model of heterogeneous rock mass considering statistical damage and its application in numerical modeling of deep roadways. Sustainability, 11(8), 2399. https://doi.org/10.3390/su11082399

MIDAS Information Technology Co. (2018) Chapter 4:Mesh. In: Midas GTS NX User Manual, 145–146.

Ng, C. W. W., Sun, H. S., Lei, G. H., Shi, J. W., & Mašín, D. (2015). Ability of three different soil constitutive models to predict a tunnel's response to basement excavation. Canadian Geotechnical Journal, 52(11), 1685-1698. https://doi.org/10.1139/cgj-2014-0361.

Oettl, G., Stark, R. F., & Hofstetter, G. (1998). A comparison of elastic–plastic soil models for 2D FE analyses of tunnelling. Computers and Geotechnics, 23(1-2), 19-38. https://doi.org/10.1016/S0266-352X(98)00015-9.

Park, K. H. (2004). Elastic solution for tunneling-induced ground movements in clays. International Journal of Geomechanics, 4(4), 310-318. https://doi.org/10.1061/(ASCE)1532-3641(2004)4:4(310).

Pinto, F. (1999). Analytical methods to interpret ground deformations due to soft ground tunneling (Doctoral dissertation, Massachusetts Institute of Technology).

Ranjbarnia, M., Zaheri, M., & Dias, D. (2020). Three-dimensional finite difference analysis of shallow sprayed concrete tunnels crossing a reverse fault or a normal fault: A parametric study. Frontiers of Structural and Civil Engineering, 14, 998-1011. https://doi.org/10.1007/s11709-020-0621-8

Rocscience. RocLab Version 1.031 (2007) Rock mass strength analysis using the Hoek–Brown failure criterion.

Rukhaiyar, S., & Samadhiya, N. K. (2016). Analysis of tunnel considering Modified Mohr-Coulomb criteria. In Recent Advances in Rock Engineering (RARE 2016) (pp. 318-326). Atlantis Press. https://dx.doi.org/10.2991/rare-16.2016.51.

Rummel, F., & Fairhurst, C. (1970). Determination of the post-failure behavior of brittle rock using a servo-controlled testing machine. Rock mechanics, 2, 189-204. https://doi.org/10.1007/BF01245574

Russo, G., Kalamaras, G. S., & Grasso, P. (1998). A discussion on the concepts of geomechanical classes behavior categories and technical classes for an underground project. Gallerie e grandi opere sotterranee, 54, 40-51.

Sarikhani Khorami M. (2012) Analysis of Geomechanical Parameters and In Situ Stress of Rock Mass in Isfahan-Shiraz Railway Tunnel Using Back Analysis Based on Displacement Monitoring. MSc Thesis, Isfahan University of Technology, Isfahan, Iran.

Shid Moosavi, S. S., & Rahai, A. R. (2018). The Performance of Integral and Semi-integral Pre-tensioned Concrete Bridges Under Seismic Loads in Comparison with Conventional Bridges. AUT Journal of Civil Engineering, 2(2), 219-226. 10.22060/ajce.2018.14338.5473

Singh, B., & Goel, R. K. (1999). Rock mass classification: a practical approach in civil engineering (Vol. 46). Elsevier.

Sulem, J., Panet, M., & Guenot, A. (1987, June). An analytical solution for time-dependent displacements in a circular tunnel. In International journal of rock mechanics and mining sciences & geomechanics abstracts (Vol. 24, No. 3, pp. 155-164). Pergamon. https://doi.org/10.1016/0148-9062(87)90522-5.

Sun, H., Liu, S., Zhong, R., & Du, L. (2020). Cross-section deformation analysis and visualization of shield tunnel based on mobile tunnel monitoring system. Sensors, 20(4), 1006.

Vitali, O. P., Celestino, T. B., & Bobet, A. (2018). 3D finite element modelling optimization for deep tunnels with material nonlinearity. Underground Space, 3(2), 125-139. https://doi.org/10.1016/j.undsp.2017.11.002.

Wang, Z., Yao, W., Cai, Y., Xu, B., Fu, Y., & Wei, G. (2019). Analysis of ground surface settlement induced by the construction of a large-diameter shallow-buried twin-tunnel in soft ground. *Tunnelling and underground space technology*, *83*, 520-532. https://doi.org/10.1016/j.tust.2018.09.021

Xing, Y., Kulatilake, P. H. S. W., & Sandbak, L. A. (2018). Investigation of rock mass stability around the tunnels in an underground mine in USA using three-dimensional numerical modeling. Rock Mechanics and Rock Engineering, 51, 579-597. https://doi.org/10.1007/s00603-017-1336-6

Xue, Y., Zhou, B., Li, S., Qiu, D., Zhang, K., & Gong, H. (2021). Deformation rule and mechanical characteristic analysis of subsea tunnel crossing weathered trough. Tunnelling and Underground Space Technology, 114, 103989. https://doi.org/10.1016/j.tust.2021.103989

Yang, H., & Xu, X. (2021). Structure monitoring and deformation analysis of tunnel structure. Composite Structures, 276, 114565. https://doi.org/10.1016/j.compstruct.2021.114565

Yasitli, N. E. (2016). Comparison of input parameters regarding rock mass in analytical solution and numerical modelling. Journal of African Earth Sciences, 124, 497-504. https://doi.org/10.1016/j.jafrearsci.2016.08.010.

Yoo, C. (2016). Effect of spatial characteristics of a weak zone on tunnel deformation behavior. Geomechanics & engineering, 11(1), 41-58. https://doi.org/10.12989/gae.2016.11.1.041.

Zhao, C., Lavasan, A. A., Barciaga, T., Kämper, C., Mark, P., & Schanz, T. (2017). Prediction of tunnel lining forces and deformations using analytical and numerical solutions. Tunnelling and Underground Space Technology, 64, 164-176. https://doi.org/10.1016/j.tust.2017.01.015.

Zheng, G., Du, Y., Cheng, X., Diao, Y., Deng, X., & Wang, F. (2017). Characteristics and prediction methods for tunnel deformations induced by excavations. Geomechanics and Engineering, 12(3), 361-397. https://doi.org/10.12989/gae.2017.12.3.361.